Ferromagnetism in tetrahedrally coordinated compounds of I/II-V elements: *Ab initio* calculations

M. Sieberer, J. Redinger, S. Khmelevskyi, and P. Mohn
Center for Computational Materials Science, Vienna University of Technology, Getreidemarkt 9/134, A-1060 Vienna, Austria
(Received 27 September 2005; published 11 January 2006)

On the basis of *ab initio* calculations employing density functional theory (DFT) we investigate half metallic ferromagnetism in zinc-blende and wurtzite compounds composed of group I/II metals as cations and group V elements as anions. We find that the formation of ferromagentic order requires large cell volumes, high ionicity and a slight hybridization of anion *p* and cation *d* states around the Fermi energy. Our calculations show that a ferromagnetic alignment of the spins is energetically always more stable than simple AF arrangements, which makes these materials possible candidates for spin injection in spintronic devices. To clarify the conditions for the flat *p*-band carrying the magnetism, we present results of a tight binding analysis.

DOI: 10.1103/PhysRevB.73.024404 PACS number(s): 75.50.Cc, 71.20.Dg, 75.50.Pp

I. INTRODUCTION

Recently, Kusakabe *et al.*[1] proposed magnetic zinc-blende CaAs as a possible material for spintronics application. Their proposal was motivated by the need for half metallic ferromagnets in spintronic devices,[2] which are seen as key ingredients. However, apart from the technological application, the magnetic I/II-V compounds represent an unusual class of ferromagnetic materials where magnetic order is carried by the anion *p* electrons without any direct involvement of *d* electrons as in the magnetic transition metals and their compounds. The *p*-electron magnetism in CaAs and the other I/II-V systems appears in the fully ordered stoichiometric compounds, and their magnetic order is intrinsic and not triggered by the presence of crystal defects of various kinds. Examples for this defect triggered *p*-electron magnetism are irradiated pyrolytic graphite containing defects[3–5] or CaB_6 doped with La.[6]

In this paper, we calculate the magnetic and electronic properties of this class of compounds. For the prototypical representative CaAs, we study the stability of the zinc-blende and wurtzite phase with respect to the true equilibrium structure and tetragonal distortions. For the possible combinations of I/II-V zinc-blende compounds we investigate the occurrance of magnetic order at the respective equilibrium volumes. The appearance of the flat band in the all-electron calculation is confirmed on the basis of a model tight-binding Hamiltonian of Slater-Koster type. We find that all I/II-V compounds have a tendency toward a ferromagnetic ground state, and the origin of the exchange is neither double exchange nor *p-d* exchange. In addition, CaAs exhibits an extremely flat, half filled band at the Fermi energy.

II. COMPUTATIONAL METHOD

The calculations were performed using the FLAIR code,[7] an implementation of the full potential linearized augmented plane wave (FLAPW) method.[8] Exchange and correlation were treated within the local density functional formalism[9] using the generalized gradient approximation of Perdew, Burke, and Ernzerhof.[10] The valence states are solutions of a semirelativistic Hamiltonian, while for core states spin-orbit coupling is included as well. To ensure converged results for the electronic and magnetic properties of all the compounds investigated, potential and charge density were expanded up to $\ell=8$ and $G_{\max}=13$ a.u.$^{-1}$. Inside the spheres the wave functions are expanded up to $\ell=8$ and a plane-wave cutoff k_{max} of $8/\min(r_{MT})$ is used, where $\min(r_{MT})$ denotes the radius of the smallest muffin-tin sphere in the cell. In calculations involving larger unit cells a k_{max} of $6/\min(r_{MT})$ turned out to be sufficiently large. A **k**-mesh sampling with $24\times24\times24$ **k** points within the full Brillouin zone was found to be satisfactory in most cases. The muffin tin radii r_{MT} were chosen as touching spheres, adapted to the approximate atomic radius to keep as much core charge inside the muffin tin sphere as possible. For comparisons of total energies, e.g., in order to optimize lattice constants, the muffin tin radii were chosen as touching spheres for the smallest volume investigated and held constant otherwise. The energy was converged better than 2.7×10^{-6} eV (10^{-7} Hartree).

III. TOTAL ENERGY

Since CaAs is the prototype of the half-metallic-ferromagnetic (HMF) systems among the II/V compounds, its total energy has been calculated for several crystal structures.

(i) The zinc-blende (ZB) structure ($I\bar{4}3m$, No. 216) consists of two interpenetrating fcc lattices, one of them shifted by the vector $\left[\frac{1}{4},\frac{1}{4},\frac{1}{4}\right]$, resulting in a two component analog of the diamond structure. Each atom of one kind is situated in an ideal tetrahedron made up of atoms of the other kind. As most semiconductors crystallize in this structure, it is of technological importance.

(ii) The wurtzite (WZ) structure ($P6_3mc$, No. 186) is the hexagonal analog to the ZB structure and has the same local environment if one assumes the ideal c/a ratio of $\sqrt{8/3}$ and internal u parameters of 3/8 for the anion site, and 0 for the cation site at the (2*b*) Wyckoff position.[11] The following discussion is based on this ideal setup.

(iii) CaAs is rather ionic and thus might favor a higher coordinated atomic arrangement in order to reduce its elec-

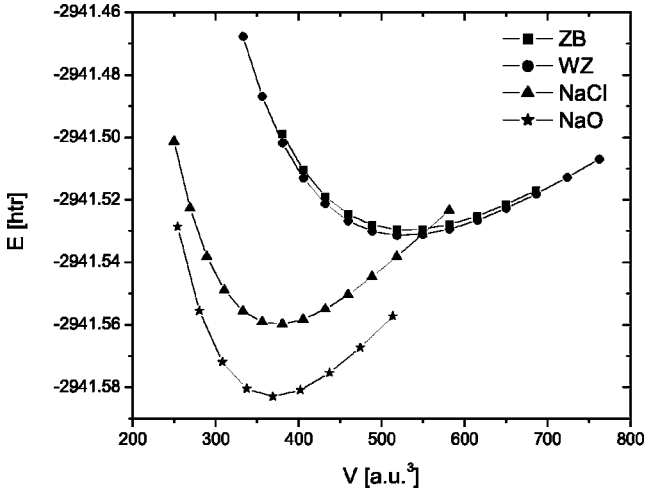

FIG. 1. Total energy for CaAs in different crystal structures. Energies and volumes are given per formula unit.

trostatic energy. For this reason also the sodium chloride (NaCl) structure ($Fm\bar{3}m$, No. 225) has been investigated. It consists of two face-centered-cubic lattices, shifted by the vector $[\frac{1}{2},\frac{1}{2},\frac{1}{2}]$, which results in an octahedral coordination for both, cation and anion.

(iv) The equilibrium modification for CaAs as reported by L'Haridon *et al.*[12] is the NaO structure ($P\bar{6}2m$, No. 189), [$a=14.84(2)$ bohr, $c=11.19(1)$ bohr], which places the As atoms in face-sharing, distorted octahedra. This structure can be derived from the ideal NiAs structure by an exchange of Ni and As atoms, a 30° rotation clockwise about the z axis, a shift of $[0,0,0.25]$ in the z direction, and finally an increase of the $a=b$ cell parameter by a factor of $\sqrt{3}$. Moreover, the symmetry is reduced due to a distortion of the Ca octahedra, which leads to an enhancement of the mean As-Ca distance by approximately 0.37%, and a reduction of the mean As-As distance by approximately 3.29% with respect to the undistorted anti-NiAs parent lattice.

To ensure that both the ZB and WZ structure are calculated with the same accuracy, the ZB structure was transformed into a translational equivalent hexagonal (or trigonal) modification ($R3m$, No. 160) (see Ref. 13). For the former, a **k** mesh of $8\times8\times4$ and for the latter a mesh with $8\times8\times6$ points was used. This ensures the same k-point density in the Brillouin zone (BZ) so that the numerical errors for different structures due to the limited set of BZ sampling points will cancel.

The calculations show (Fig. 1) that the compounds with the octahedral coordination for the anion, like those in NaCl and NaO, are energetically favored. They have a smaller cell volume and a higher bulk modulus, indicating that the bonding is stronger due to the smaller interatomic distances. The experimentally observed NaO structure has indeed the lowest total energy, the calculated lattice constant of 15.03 bohr is in good agreement with the experimentally found value of 14.89 bohr. If one starts a calculation with the corresponding ideal anti-NiAs structure and allows for a relaxation of the atoms, the distortion found is less pronounced as in experiment, and reduces the total energy only slightly (by

TABLE I. Cell volume V/f.u., bulk modulus B, magnetic moment M per f.u., band gap at E_F for spin-up/spin-down, and spin splitting ΔE for CaAs in different crystal structures.

	ZB	WZ	NaO	NaCl
V (bohr^3/f.u.)	531	523	369	374
B (GPa)	26	26	46	41
M (μ_B/f.u.)	1	1	0	0
Gap (eV)	2.78/2.30	2.80/2.30	0	0
ΔE (eV)	0.58	0.58	0	0

≈16 meV/f.u.). The comparison of ZB and WZ structure shows that the hexagonal arrangement is lower in energy by approximately 46 meV/f.u., but both exhibit HMF. In contrast to that, CaAs in the NaO as well as the NaCl arrangement is nonmagnetic and metallic at the equilibrium cell volume. Table I lists the cell parameters, the bulk modulus B (determined from a Murnaghan equation fit[14]), the magnetic moment M, the energy gap, and the spin splitting.

Recently, Geshi *et al.*[15] investigated the stability of half metallicity in the ZB structure against tetragonal distortion. They fixed the cell volume to the ZB equilibrium and found two local minima in the total energy for a c/a ratio of ≈1.47 and 0.66, respectively, where only for the latter half metallicity occurred. The results of a more detailed calculation, including a variation of the cell volume V for each c/a, are shown in Fig. 2. Our results are only in partial agreement with the findings of Geshi *et al.*,[15] insofar as the cubic structure ($c/a=1$) is always at a local maximum in energy, but there is no stable solution within the half metallic regime. This becomes evident by comparing the total energy surface with the magnetic moment contour plot in the center panel of Fig. 2. We find that HMF is present near the cubic symmetry, but vanishes for increasing tetragonal distortion and in general becomes favored only for large cell volumes. The dots crossing the HMF regime mark the equilibrium cell volume at a given c/a ratio. We find that half metallicity is found for $0.8\lesssim c/a\lesssim1.15$, and that the maximum energy gain within the HMF regime due to the distortion is 0.15–0.2 eV/f.u. In the right panel of Fig. 2, the lowest energy for each c/a ratio is shown. There exists a local (nonmagnetic) minimum around 1.55, in the limit of small c/a, no stable solution has been found within the investigated c/a range. The total energy of the WZ structure with an ideal (ZB-equivalent) crystallographic arrangement is also at a local energy maximum so that it shows a similar behavior to the ZB structure occurs.

These results show that the ground state of CaAs found experimentally is energetically rather far away (≈1.4 eV/f.u.) from the structures which are expected to exhibit HMF. Nevertheless, a preparation as a thin film on a substrate may be possible. Due to the large lattice constant of CaAs, suitable substrates are not widely available. Suggesting such substrates with any degree of certainty goes beyond the capabilities of this theoretical investigation. However, the occurrance of p-electron magnetism in these materials clearly distinguishes them from the transition-metal pnictides and chalcogenides[13,16,17] where the transition metals carry the magnetic moments. In the present system the magnetic

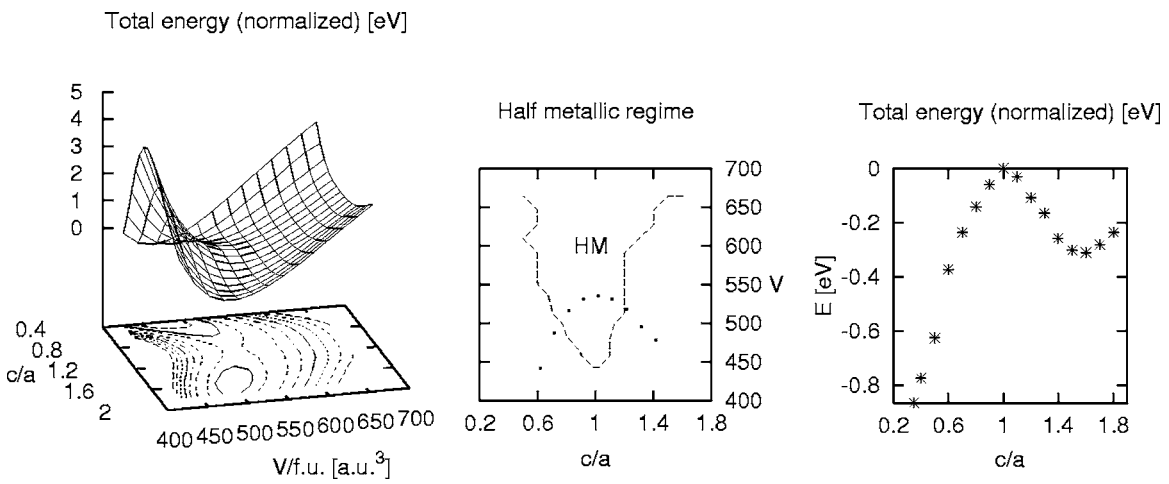

FIG. 2. Left panel: total energy for CaAs in a tetragonal distorted ZB structure for various values of c/a and volume V/f.u. Center panel: The dashed line marks the existence region of HMF solutions in the c/a vs V plane; the dotted line denotes the equilibrium cell volume for a given c/a ratio. Right panel: total energy as a function of c/a and the respective equilibrium volume (minimal energy path in the c/a vs V plane).

moments appear in the anion p-band, and therefore makes them a technologically challenging research area.

IV. MAGNETISM IN II-V ZINC-BLENDE COMPOUNDS

In the following detailed investigation we present our results for the ZB structure; however, due to their close similarity, an equivalent behavior can be expected for the respective compounds in the WZ structure. The half metallic ferromagnets ZB-CaX with X=P, As and Sb exhibit a magnetic moment of $1\mu_B$, caused by a curious, almost dispersionless band (see Fig. 3).[1] The band structure for CaAs (a_0=12.86 bohr) is shown in Fig. 3, the site and orbital projected density of states (DOS) is given in Fig. 4. It has been argued that the reason for this flat band is a mixing of Ca t_{2g} and As p-like states, and that the flat band is essential for the HMF. In order to study the mechanism behind this phenomenon and to explore other candidates for half metallicity, several other combinations of group II elements with group V elements have been investigated, Table II lists the results for the ground states and the respective equilibrium lattice constants a_0.

It is remarkable how widespread HMF is found within this class of compounds. All representatives having Ca, Sr, or Ba as cations exhibit HMF, additionally also MgN. All have in common that their band structure exhibits a gap separating the anion and the cation states. This feature is different for the 3d pnictides, where the gap appears only in the minority

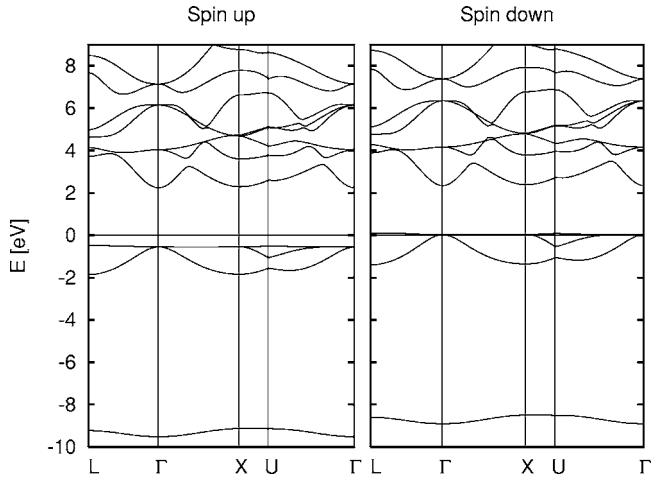

FIG. 3. Band structure of ZB-CaAs for both spin channels.

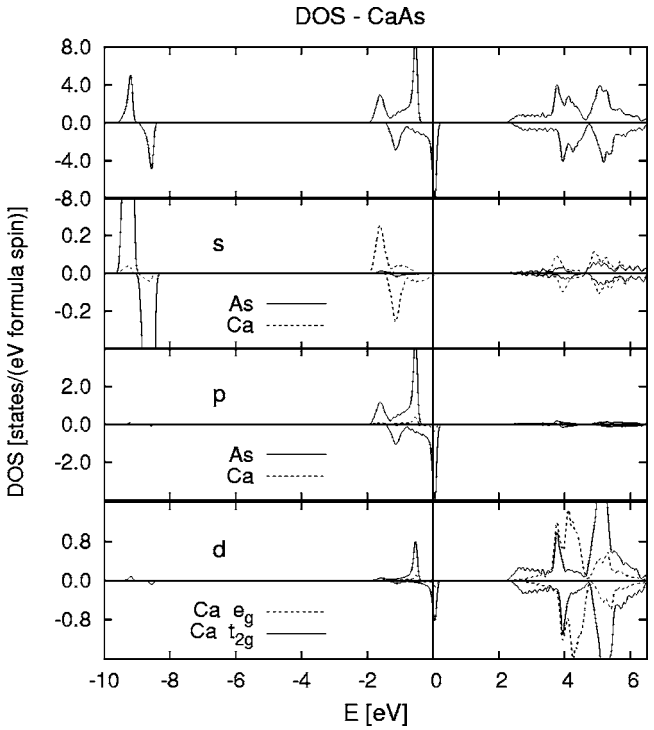

FIG. 4. Orbital and symmetry projected DOS of ZB-CaAs. The main contribution at E_F comes from As-p, with a small admixture from Ca-d (t_{2g}) and Ca-p.

TABLE II. Left part: Ground state calculated at the equilibrium lattice constants a_0 for several II-V compounds in the ZB structure. "+' denotes a half metallic, "−" a nonmagnetic metallic ground state, and "*m*" a system at the verge of a magnetic state. Right part: equilibrium lattice constants (given for an fcc unit cell containing four formula units) for the various systems investigated.

	Ground state				Lattice constant a_0 (bohr)			
	N	P	As	Sb	N	P	As	Sb
Be	−	−	−	−	7.49	9.38	9.82	10.69
Mg	+	*m*	*m*	−	9.15	11.16	11.54	12.45
Ca	+	+	+	+	10.57	12.45	12.86	13.71
Sr	+	+	+	+	11.34	13.29	13.62	14.55
Ba	+	+	+	+	12.20	14.11	14.43	15.37

states, an asymmetry which is caused by the large exchange splitting of the *d* bands.[18]

For the half metallic compounds investigated here, a_0 varies in a wide range between 9.15 bohr for MgN to 15.37 bohr for BaSb. Compared to conventional ZB III-V semiconductors with values up to 12.25 bohr (CdTe), the II-V compounds tend toward large interatomic spacings, which can be attributed to the comparably big cations. Thus the lighter representatives such as MgN or CaN having lattice constants in a physically reasonable range, might be of great technological importance and will warrant further experimental investigation.

A. The origin of magnetism

As expected, all HMF compounds investigated exhibit a magnetic moment M of $1\mu_B$ per formula unit. This integer value comes about because, for the majority spin direction, the Fermi energy E_F is situated within a gap, which means that the bands below are occupied by an integer number of spin-up electrons. Since the total number of electrons is an integer as well, a resulting magnetic moment has to be an integer, too. The magnitude of the magnetic moment can be determined by the $|(8\text{-}n)|$ rule, where n denotes the total number of valence electrons per formula unit. In other words, the rather localized anion *p* band is completely filled with the exception of one hole, which is responsible for the magnetic moment of $1\mu_B$. Comparing Tables III and II, one finds a clear correlation between the DOS at E_F and the ground state of the corresponding compound. A high DOS at the Fermi energy—in these compounds created by a narrow anion *p* band—appears to be sufficient to cause an instability of the non-magnetic state within the framework of the Stoner criterion. The application of this criterion is justified, because in the nonmagnetic state, all these compounds are good metals. However, the criterion itself does not say anything about the type of magnetism which might appear in the magnetically ordered equilibrium state. In the present case the magnetic state is, however, not an itinerant electron state but rather a localized one where the unpaired spins are located in well defined orbitals. The flat band magnetism appearing in this class of compounds can be seen as the magnetism of unpaired electrons occupying an atomic like state, which in the language of band structure appears as a flat (undispersed) band. The resulting magnetic band splitting is much larger than the respective band width, which is a typical sign for a well localized magnetic moment.

TABLE III. DOS at E_F assuming a hypothetical nonmagnetic state.

	$N(E_F)$ states/(eV f.u.)			
	N	P	As	Sb
Be	1.30	1.16	1.17	1.19
Mg	3.47	2.39	2.28	1.10
Ca	5.30	5.52	5.38	5.17
Sr	5.10	5.64	5.70	5.79
Ba	4.52	5.23	5.55	5.64

MgP and MgAs ($M \approx 0.08$ and $0.02\mu_B$/f.u.) are the boarderline cases where the DOS value is on the verge of producing a spin splitting, which is smaller than the width of the *p*-band, so that in the magnetic state both spin channels have a nonvanishing DOS at E_F. These systems are typical for itinerant electron magnetism with small magnetic moments and a magnetic band splitting which is smaller than the respective band width. For all II/V compounds investigated the magnetic moment can be attributed mainly to the anion (0.6 to $0.8\mu_B$/atom), the cation plays only a minor role. The cation moment is always aligned parallel to that of the anion and always smaller than $0.1\mu_B$/atom. The relatively large contribution of the interstitial region to magnetism is typical for a structure with large voids. A plot of the charge and spin density of CaAs is shown in Fig. 5. The spin density is well localized at the As site, whereas everywhere else only a small diffuse induced spin-density occurs.

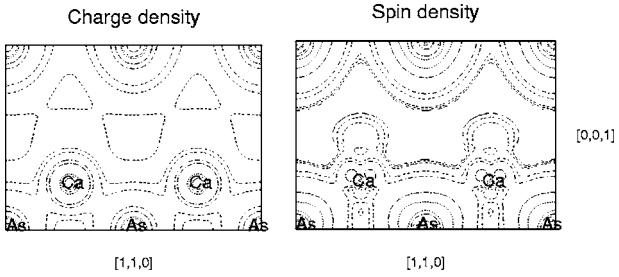

FIG. 5. Charge and spin density of CaAs in the ZB structure within the [1,1,0] plane in the fcc cell.

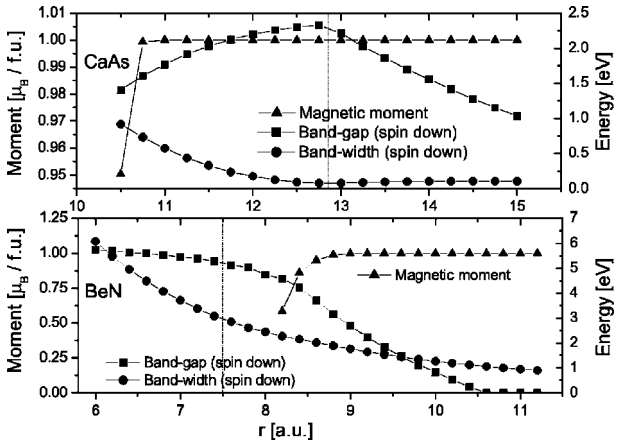

FIG. 6. Comparison of the magnetic moment, the width of the gap, and the maximum bandwidth of the anion p-like band along the path L-Γ-X-U-Γ for CaAs and BeN. The vertical line marks the equilibrium lattice constant.

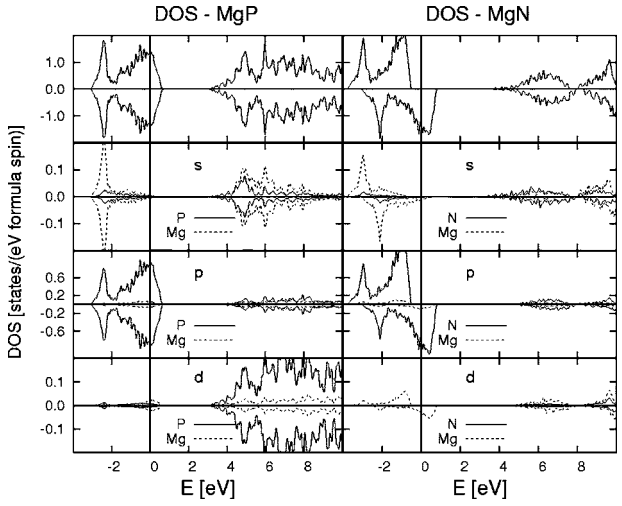

FIG. 7. Total, site, and symmetry projected DOS for MgP and MgN. In both calculations the muffin tin radii r_{MT} were chosen as touching spheres and r_{MT} of Mg was set to 2.2 bohr.

The mechanism for this parallel alignment between the anion and the cation moment can be understood in terms of the model of covalent polarization.[19] The cation states mix weakly with the flat anion p band, which is spin split and almost of equal shape in both spin channels. As the hybridization is of similar strength for both spin directions, the cation has fewer occupied states in the spin down channel, which results in a parallel polarization of the latter. This becomes evident by inspecting the orbital-projected DOS in Fig. 4: There are fewer Ca-d states below E_F in the minority than in the majority direction.

Recapitulating, two simple conditions have to be fullfilled in order to have HMF present in the ZB structure: (i) there must exist a gap between anion and cation states and (ii) the band at the Fermi energy must be flat. In this case, the spin splitting will automatically shift the majority states below E_F and create HMF.

B. Volume dependence of HMF

Since the cell volume controls the dispersion of the electronic bands it has probably the largest influence on the formation of HMF. Figure 6 compares the magnetic moment, the energy gap, and the bandwidth along the path L-Γ-X-U-Γ for CaAs and BeN versus the fcc lattice constant a. CaAs has been chosen as a typical representative of the heavier compounds, while BeN is nonmagnetic and the lightest system investigated. The magnetic moment of CaAs is surprisingly stable, it retains its integer value down to a cell volume of 58% from its equilibrium. BeN, on the contrary, becomes half metallic only if the cell volume is increased by 62%, a volume change which is probably beyond physical realizability. This behavior is not surprising as it also has been found among the 3d pnictides, e.g., in CrAs.[20] For BeN, the bandwidth of the anion p-like band at E_F is reduced with increasing interatomic separation, which explains the HMF state appearing at $a \approx 8.8$ bohr. The trend is the same for CaAs, which, however, has an initially much smaller bandwidth.

The behavior of the electronic gap has been studied, too. Coming from large volumes it first increases due to the repulsion of anion and cation states. This effect becomes increasingly reduced (BeN) or even overcompensated (CaAs) by the broadening of the bands forming the gap. The gap values plotted represent the smallest value along the path L-Γ-X-U-Γ, irrespectively whether they were due to a direct or an indirect gap.

C. Ionicity

Another quantity that plays an important role for magnetism is the ionicity of the compound. This can be seen best if one investigates the nonmagnetic to magnetic transition by a stepwise increase of the anion-electronegativity, e.g., in the series MgX with X=As, P, and N. Even though the cell volume is smallest for MgN, it is the only magnetic compound in this series. This behavior is due to the stronger localization of the N 2p states compared to the P 3p states. In Fig. 7, the site and symmetry projected DOS for MgP and MgN is compared. In both cases the admixture of cation states at E_F is negligible, but there is a difference in the shape of the anion p orbital, resulting in a clearly higher DOS at E_F for MgN.

The ionicity also has an influence on the energy gap. Table IV lists type (direct or indirect) and magnitude of the gap for the II-V compounds investigated. As discussed in the previous section, the gap becomes increasingly smaller for systems with large lattice constants because the energy bands retain their atomic energies due to the weakened repulsion between anion and cation states. The ionicity is thus responsible for the exceptional position of BeN, which has the largest gap of all.

D. The importance of d orbitals at the cation

Along the series XAs with X=Ca, Mg, and Be, the ionicity variation is not strong as is the case for MgX discussed at the beginning of the preceding section. However, there is a

TABLE IV. Energy gap in (eV *d*, direct, *i*, indirect); for magnetic members + denotes spin up and − spin down.

	Energy gap [eV]			
	N	P	As	Sb
Be	8.07/5.32 (*d*/*i*)	3.79/1.63 (*d*/*i*)	3.69/1.45 (*d*/*i*)	2.92/1.26 (*d*/*i*)
Mg	3.86/2.82 (+*d*/−*d*)	2.61/2.50 (+*i*/−*i*)	2.08/2.05 (+*d*/−*d*)	1.91 (*d*)
Ca	3.2/2.17 (+*i*/−*i*)	2.96/2.42 (+*i*/−*i*)	2.72/2.23 (+*i*/−*i*)	2.67/2.26 (+*i*/−*i*)
Sr	2.45/1.37 (+*i*/−*i*)	2.62/2.10 (+*i*/−*i*)	2.27/1.77 (+*i*/−*i*)	2.32/1.92 (+*i*/−*i*)
Ba	2.13/1.08 (+*i*/−*i*)	2.31/1.80 (+*i*/−*i*)	2.04/1.56 (+*i*/−*i*)	2.09/1.70 (+*i*/−*i*)

clear difference between the bonding in CaAs and MgAs, which cannot be explained by the small volume change (Fig. 8). These differences in bonding are a consequence of the *d* orbitals, which in the case of Ca are energetically close enough to the anion bands for a hybridization to occur.

This hybridization leads to an anomalously flat anion *p* band near E_F, a more detailed discussion in the scope of a tight binding calculation is given in a later section. Even though these *d* orbitals favor this type of flat band magnetism, their presence is not conditional for the described mechanism of HMF. For example, in the case of MgN, which is a HMF, they play a negligible role. Furthermore, the comparison of the band structure of CaAs and hypothetical fcc As for the same lattice constant, which was suggested by Kusakabe *et al.*,[1] in fact shows a broader band for fcc As. In addition to the results shown by Kusakabe *et al.*,[1] it should be pointed out that fcc As at this volume is magnetic anyway. On the other hand, the hybridization with the *d* states can induce a magnetic state into compounds that otherwise would become magnetic only at larger, often unphysical lattice constants.

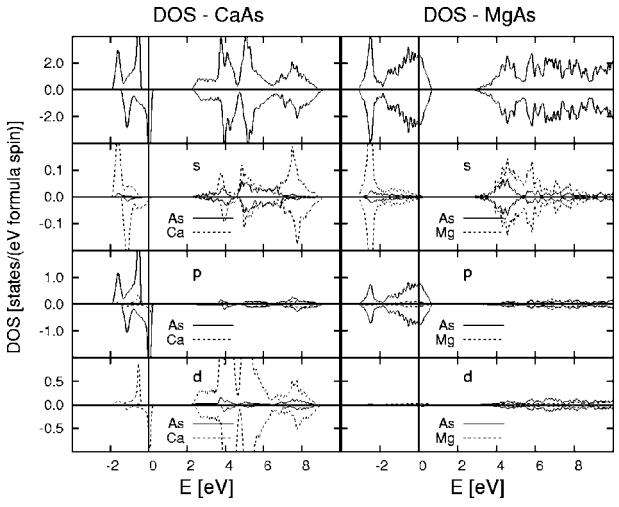

FIG. 8. Total, site, and symmetry projected DOS for CaAs and MgAs.

TABLE V. Total energy difference in meV/f.u. between FM and AFM ground state ($\Delta_1 = E_{AFM} - E_{FM}$) and between FM and a hypothetical nonmagnetic state ($\Delta_2 = E_{NM} - E_{FM}$). The resulting values are given as Δ_1/Δ_2.

	N	P	As	Sb
Be	0	0	0	0
Mg	114/189	≈0	≈0	0
Ca	92/222	71/123	70/178	60/80
Sr	96/189	67/118	64/111	58/93
Ba	90/166	56/77	49/71	63/63

E. Stability of FM versus AFM order

In order to estimate the stability of the FM against a simple antiferromagnetic (AFM) alignment of the spins, the II-V compounds were investigated in an eight atom cell with cubic primitive lattice vectors and a layer geometry along the [0,0,1] direction. Two anions are situated in the $z=0$ plane, two in the plane $z=a/2$, which can be assumed during the calculation to have an antiparallel magnetization. Table V lists the calculated total energy differences between the nonmagnetic (NM), the FM, and a possible AFM solution. In all magnetic cases, the FM alignment is most stable, followed by AF, and finally by the nonmagnetic solution. In general, the materials containing light elements show higher energy differences, probably because their bonding is more direction-dependent leading to a stronger inter-atomic exchange. Even though the corresponding values for the 3*d*-metal-pnictides are two or three times larger,[16] the results found here are remarkable considering that they come from *p*-electron exchange.

Motivated by earlier investigations[21] on magnetic stability of fcc alloys, we tried to estimate the paramagnetic Curie temperature. To this end we performed spin-spiral calculations[22] employing the augmented spherical wave (ASW) method[23] for CaAs along two directions in **k**-space. We find (see Fig. 9) a smooth variation of the total energy as

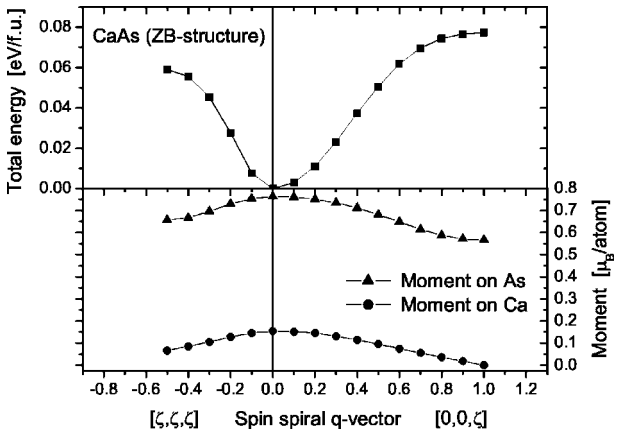

FIG. 9. Upper panel: total energy as a function of the spin spiral in $[\zeta,\zeta,\zeta]$ and $[0,0,\zeta]$ direction, respectively. The spin spiral propagation vector **q** is given in multiples of $2\pi/a$. Lower panel: magnetic moment of Ca and As.

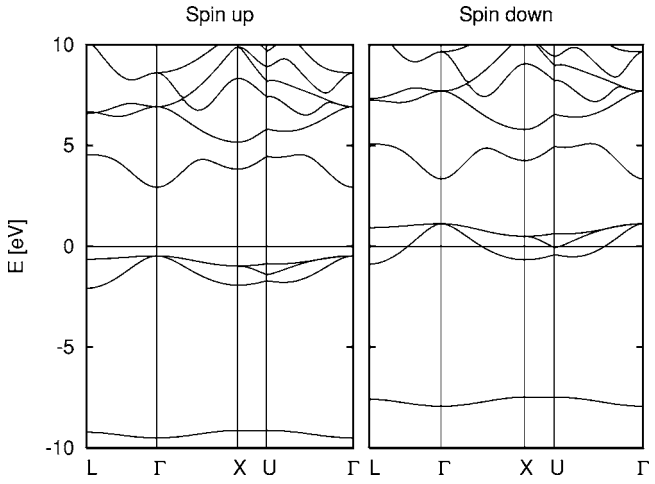

FIG. 10. Bandstructure of NaP.

a function of the spin spiral **q** vector with an energy minimum at the FM case $\mathbf{q}=[0,0,0]$. The value $\mathbf{q}=[0,0,1]$ describes a spin ordering of the AFI type and $\mathbf{q}=[0.5,0.5,0.5]$ one of the AFII type. For the definition of AFI and AFII spin ordering in the fcc lattice see Ref. 21 In the mean field approximation the paramagnetic Curie temperature Θ can be written as

$$k_B\Theta = \frac{1}{8}(3\Delta E_1 + 4\Delta E_2). \quad (1)$$

In Eq. (1) we assume a spin of $S=1/2(1\mu_B)$ and first nearest neighbor interaction on a anion fcc sublattice only. $\Delta E_1 = E(\mathrm{AFI}) - E(\mathrm{FM}) = 77$ meV and $\Delta E_2 = E(\mathrm{AFII}) - E(\mathrm{FM}) = 59$ meV. The resulting paramagnetic Curie temperature amounts to $\Theta = 680$ K, which would be a temperature well suited for technological application. The magnitude of ΔE_1 from the ASW calculation is in fair agreement with the FLAPW results. The size of the magnetic moment (lower panel of Fig. 9) changes only slightly for different spin propagation vectors, which can be expected for a localized moment.

V. ZB COMPOUNDS CONTAINING ALKALI METALS

From the analysis given above one can expect HMF also among I/V compounds if the ZB structure is assumed. Even though no investigation toward their structural stability has been made, some of them have been investigated simply for the sake of interest. In all cases the magnetic moment is $2\mu_B$, because there are two electrons missing in the anion p band instead of 1 for the group II elements. Since the alkali s levels are situated at higher energies than those of the alkaline earth elements, the ionicity is slightly increased, thus already NaP is half metallic, whereas the analog MgP is not. LiP as well as LiAs are not listed because they are nonmagnetic. The band structure of NaP as a representative can be seen in Fig. 10. It is analogous to that of the II–V compounds, the high DOS at E_F is again the reason for the occurrance of the spin splitting. All systems listed in Table VI exhibit a direct gap at the center of the Brillouin zone Γ.

TABLE VI. Half metallic members among the alkali-pnictides in the ZB structure. Listed are the optimized lattice constant a_0, the bulk modulus B, the magnetic moment per f.u. M/f.u., the width of the gap along L-Γ-X-U-Γ for the spin-up/spin-down channel, the magnetic band splitting E_m and the energy difference $\Delta_1 = E_{AFM} - E_{FM}$ and $\Delta_2 = E_{NM} - E_{FM}$ per f.u.

	KAs	KP	NaAs	NaP	LiN
a_0 (bohr)	14.87	14.57	12.91	12.58	8.86
B (GPa)	8.6	8.9	11.0	12.0	38.2
M/f.u. (μ_B)	2	2	2	2	2
Gap (eV)	2.81/1.76	3.21/2.08	2.8/1.6	3.4/2.23	6.77/4.68
E_m (eV)	1.33	1.44	1.41	1.54	2.66
Δ_1/Δ_2 (meV)	107/514	96/582	102/248	119/345	212/688

VI. THE FLAT BAND

The so-called flat band responsible for the instability toward magnetic ordering is mainly anion p-like and located around E_F. Symmetry considerations allow to draw some conclusions in advance. The center of the Brillouin zone, Γ, has the full symmetry of the crystal $T_d(\bar{4}3m)$ and hence only mixing between As p and Ca t_{2g} states belonging to the same representation T_2 occurs. Along the direction Λ (Γ to L), symmetry reduces to $3m$, and one p band splits off toward lower energies due to s-p_z and p_z-p_z hybridization creating a second peak in the DOS at approximately -1.6 eV (spin up) (see, e.g., Fig. 4). A further lifting of the remaining degeneracy in the p-band close to E_F occurs, e.g., at U ($mm2$ symmetry), where p_y-d_{yz}, p_x-d_{xz}, and p_z-s-e_g mixing is allowed. For a better understanding of the nature of the flat-band a tight binding (TB) analysis of Slaterle-Koster type

TABLE VII. Tight binding parameters for CaAs given in units of eV.

	$V(ss)$	$V(sp)$	$V(pp\sigma)$	$V(pp\pi)$	$V(sd)$	$V(pd\sigma)$	$V(pd\pi)$
As-Ca	−0.37	0.48	1.42	−0.35	−0.55	−1.03	0.48
Ca-As		0.97					
Ca-Ca	−0.16	0.21	0.37	−0.09			
As-As	−0.012	0.09	0.16	−0.04			
On site	As(s)	As(p)	Ca(s)	Ca(d)	Ca(p)		
Energy	−8.3	0.65	3.8	4.0	10.0		

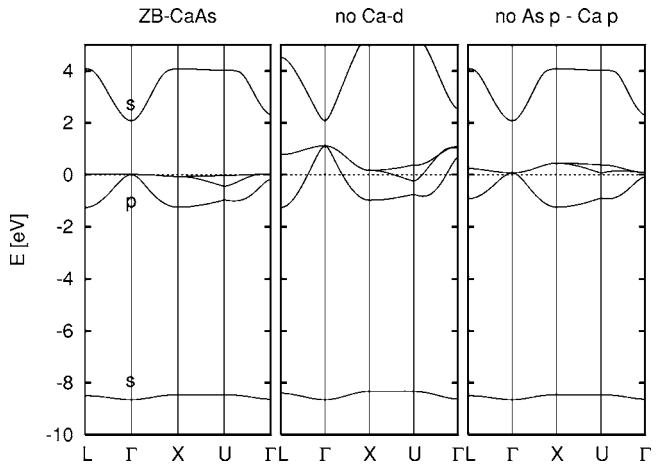

FIG. 11. Model tight binding (TB) band structure containing the five lowest bands, plotted along the **k** points L-Γ-X-U-Γ. Left panel: full TB simulation; center panel: p-d interaction switched off; right panel: p-p interaction switched off.

has been performed.[24] Nearest and next nearest neighbor (s,p) interactions suffice to yield a satisfactory agreement with the DFT FLAPW results, provided that Ca-d states take part in the Ca-As interaction, whereas Ca d-d interactions may be neglected. The TB parameters, i.e. interatomic matrix elements and on-site energies, are given in Table VII. They were obtained in the following way: Parameters for the next nearest neighbor (s,p) interaction (As-As and Ca-Ca) were determined from the respective As and Ca fcc DFT FLAPW sublattice band structures calculated at the CaAs lattice constant. The on-site energies have been chosen in accordance to the respective band centers of the CaAs DFT FLAPW band structure. Analogous to the next nearest neighbor (As-As, Ca-Ca) interactions, all nearest neighbor Ca(s,p)-As(s,p) matrix elements were chosen to correctly reproduce the rather narrow As-s band at ≈ -9 eV and the width of the anion p band. In all cases the ratio between π and σ interactions both for p-p and p-d bonding was set according to Harrison.[25] Concerning the As (s,p)-Ca d interaction, its value could be reduced if Ca d-Ca d interactions are included. These interactions broaden the Ca-d bands and thus also increase the p-d interaction.

The TB band structure calculated for the symmetry L-Γ-X-U-Γ containing the five lowest lying bands is shown in the left panel of Fig. 11 and is in good agreement with the FLAPW results, as already stated above. The other two band structures in Fig. 11 have been calculated by switching off the d orbitals on Ca and the As p-Ca p mixing, respectively. Quite clearly, the Ca-p As-p interaction generates a dispersion of the flat band with a trend opposite to the one caused by the Ca-d As-p interaction. For the existence of the magnetically active flat band, this means that the influences of both interactions cancel each other, rendering one anion p-band dispersionless.

The same differences in the p-p and p-d interaction also explains the negative curvature of the uppermost p band at Γ for compounds with mainly or exclusively s-p-like interactions (e.g., ordinary semiconductors such as InSb), and the positive one if p-d interaction dominates, as it is the case for some 3d pnictides like CrAs or MnBi (Refs. 20 and 26) whose minority band structure is at least partially comparable to those of the II/V compounds because all d states are situated well above the gap.

Since the magnetism in all these compounds relies on the existence of a flat anion p-band, they might serve as examples for the flat band (ferro-) ferrimagnetism, which has been proposed on the basis of the Hubbard model.[27] Rigorous examples of ferromagnetism (or ferrimagnetism) in the Hubbard model—at least in the past—have been limited to singular models with infinite Coulomb interaction U,[28] or systems in which the magnetization is supported by a nearly flat[29,30] band (large ratio U/W). Within the Hartree- Fock approximation the Hubbard and the Stoner models become equivalent so that the Hubbard U can be determined from the magnetic splitting of the flat band. Given a flat band dispersion of about $W=0.07$ eV yields the ratio U/W to be about 12, much larger than for ordinary d-electron magnets.

VII. CONCLUSION

We find that half metallicity is very common among ionic compounds composed of alkaline earth/alkali metals and group V elements if a tetrahedrally coordinated crystal structure like the ZB or WZ structure is assumed. Magnetic order is favored by large lattice constants, high ionicity, and empty 3d orbitals present on the cation like in CaAs. The resulting spin splitting yields a half metallic state, because a gap is always present in both spin channels. The origin of ferromagnetic order of these materials depends on the appearance of a flat p-electron band at the Fermi energy in the fully ordered compound. This is in contrast to most other magnetic semiconductors (e.g., Mn-doped GaAs, Mn-doped chalcopyrites), where magnetic transition metal impurities are inserted into a semiconductor host. Employing a tight-binding model, we show that the flat anion p band is a property of the crystal structure and its formation depends on the nearest neighbor s-p and p-d interaction. Calculations of the total energy show that this class of materials exists as bulk phases at best in metastable form. However, their highly interesting magnetic properties, including a reasonably large Curie temperature, might warrant experimental efforts to stabilize these materials in a fourfold coordinated structure such as ZB or WZ (e.g., via vacuum laser deposition) on suitable substrates.

[1] K. Kusakabe, M. Geshi, H. Tsukamoto, and N. Suzuki, J. Phys.: Condens. Matter **16**, 5639 (2004); see also cond-mat/0402641 (unpublished).
[2] J.-H. Park, E. Vescovo, H.-J. Kim, C. Kwon, R. Ramesh, and T. Venkatesan, Nature (London) **392**, 794 (1998).
[3] P. Esquinazi, D. Spemann, R. Höhne, A. Setzer, K.-H. Han, and T. Butz, Phys. Rev. Lett. **91**, 227201 (2003).
[4] K. Kusakabe and M. Maruyama, Phys. Rev. B **67**, 092406 (2003).
[5] P. O. Lehtinen, A. S. Foster, Yuchen Ma, A. V. Krasheninnikov, and R. M. Nieminen, Phys. Rev. Lett. **93**, 187202 (2004).
[6] Zhigang Wu, D. J. Singh, and R. E. Cohen, Phys. Rev. B **69**, 193105 (2004).
[7] http://www.uwm.edu/weinert/flair.html
[8] E. Wimmer, H. Krakauer, M. Weinert, and A. J. Freeman, Phys. Rev. B **24**, 864 (1981).
[9] W. Kohn and L. J. Sham, Phys. Rev. **140**, A1133 (1965).
[10] J. P. Perdew, K. Burke, and M. Ernzerhof, Phys. Rev. Lett. **77**, 3865 (1996).
[11] http://cst-www.nrl.navy.mil/lattice/struk/b4.html
[12] P. L'Haridon, J. Guyader, and M. Hamon, Revue de Chimie minerale **13**, 185 (1976).
[13] M. S. Miao and W. R. L. Lambrecht, Phys. Rev. B **71**, 064407 (2005).
[14] F. D. Murnaghan, Proc. Natl. Acad. Sci. U.S.A. **30**, 244 (1944).
[15] M. Geshi, K. Kusakabe, H. Tsukamoto, and N. Suzuki, *A new ferromagnetic material excluding transition metals: CaAs in a distorted zinc-blende structure*, AIP Conf. Proc. No. 772 (AIP, Melville, NY, 2005), p. 327.
[16] B. Sanyal, L. Bergqvist, and O. Eriksson, Phys. Rev. B **68**, 054417 (2003).
[17] Wen-Hui Xie, Bang-Gui Liu, and D. G. Pettifor, Phys. Rev. B **68**, 134407 (2003).
[18] R. A. de Groot, F. M. Mueller, P. G. van Engen, and K. H. J. Buschow, Phys. Rev. Lett. **50**, 2024 (1983).
[19] P. Mohn, *Magnetism in the Solid State*, Springer Series in Solid-state Sciences, Vol. 134 (Springer, Heidelberg, 2003).
[20] I. Galanakis and P. Mavropoulos, Phys. Rev. B **67**, 104417 (2003).
[21] J. Kübler, A. R. Williams, and C. B. Sommers, Phys. Rev. B **28**, 1745 (1983).
[22] L. M. Sandratskii, Phys. Status Solidi B **135**, 167 (1986).
[23] A. R. Williams, J. Kübler, and C. D. Gelatt, Jr., Phys. Rev. B **19**, 6094 (1979).
[24] J. C. Slater and G. F. Koster, Phys. Rev. **94**, 1498 (1954).
[25] W. A. Harrison, *Electronic Structure and the Properties of Solids* (W. H. Freeman and Company, San Francisco, 1980).
[26] Y.-Q. Xu, B.-G. Liu, and D. G. Pettifor, Phys. Rev. B **66**, 184435 (2002).
[27] E. H. Lieb, Phys. Rev. Lett. **62**, 1201 (1989).
[28] Y. Nagaoka, Phys. Rev. **147**, 392 (1966).
[29] H. Tasaki, Phys. Rev. Lett. **75**, 4678 (1995).
[30] A. Mielke, Phys. Rev. Lett. **82**, 4312 (1998).